

## Original Article

# Connexin36 localization along axon initial segments in the mammalian CNS

Deepthi Thomas<sup>1\*</sup>, Joanne MM Senecal<sup>1\*</sup>, Bruce D Lynn<sup>1</sup>, Roger D Traub<sup>2</sup>, James I Nagy<sup>1</sup>

<sup>1</sup>Department of Physiology and Pathophysiology, Max Rady College of Medicine, University of Manitoba, Winnipeg, Canada; <sup>2</sup>AI Foundations, IBM T.J. Watson Research Center, Yorktown Heights, NY, USA. \*Equal contributors.

Received November 17, 2020; Accepted December 3, 2020; Epub December 15, 2020; Published December 30, 2020

**Abstract:** Electrical synapses formed by gap junctions occur at a variety of neuronal subcellular sites in the mammalian central nervous system (CNS), including at somatic, dendritic and axon terminal compartments. Numerous electrophysiological studies using mice and rats, as well as computer modelling approaches, have predicted the additional occurrence of electrical synapses between axons near their emergence from neuronal somata. Here, we used immunofluorescence methods to search for localization of the neuronal gap junction-forming protein connexin36 (Cx36) along axon initial segments (AISs) labelled for the AIS marker ankyrinG. Immunofluorescent Cx36-puncta were found to be associated with AISs in several CNS regions of mice, including the spinal cord, inferior olive and cerebral cortex. Localization of Cx36-puncta at AISs was confirmed by confocal single scan and 3D imaging, immunofluorescence intensity profiling and high resolution structured illumination microscopy (SIM). AISs measuring up to 30 µm in length displayed typically a single Cx36-punctum and the incidence of these long AISs displaying Cx36-puncta ranged from 3% to 7% in the inferior olive and in various layers of the cerebral cortex. In the inferior olive, the gap junction associated protein zonula occludens-1 (ZO-1) was found to be co-localized with Cx36-puncta on AISs, indicating that these puncta have some of the molecular constituents of gap junctions. Our results add to the neuronal subcellular locations at which Cx36 is deployed, and raise possibilities for its involvement in novel functions in the AIS compartment.

**Keywords:** Electrical synapses, neuronal gap junctions, electrical coupling

## Introduction

Electrical synapses formed by gap junctions between neurons are now recognized to serve as key circuit elements for mediation of neuronal communication and to have essential and divergent functional roles in a variety of regions in the mammalian CNS [1-3]. The vast majority of these gap junctions are composed of Cx36 that forms intercellular channels and which is associated with various structural and regulatory proteins that are thought to contribute to the complex operational features of electrical synapses [4, 5]. The types of neurons between which electrical synapses occur, both during development and in the mature CNS, are diverse and include inhibitory interneurons and long projection excitatory neurons [6]. The subcellular sites at which these synapses are deployed between neuronal elements are equally varied, ranging from their occurrence at

distal vs. proximal dendrites, between dendrites and neuronal somata and between neuronal somata, forming “purely” electrical synapses [6]. Neuronal gap junctions also occur between nerve terminals and postsynaptic structures, forming “mixed” chemical/electrical synapses [7, 8]. Another interesting site of gap junctions forming electrical synapses is directly between axons, either near or at some distance from neuronal somata. This has been found in various species of fish [9, 10]. In the mammalian CNS, the possibility of gap junction-mediated electrical coupling between axons has been the subject of numerous reports [reviewed in 11, 12]. For example, there is substantial literature on the role of hypothesized axonal gap junctions in high-frequency electrical network activity [13], such as transiently-stable patterns of electrical activity that appear to be generated and maintained by oscillatory states in neuronal assemblies. The mechanisms responsible

for production of these states are not fully known. However, experimental data and modelling studies have provided compelling predictions for their mediation by electrical synapses that have been proposed to link axons of principal cells in the cerebral cortex and those in the hippocampus, with the proposed axonal gap junctions estimated to occur within ~150 µm of neuronal somata [13-15]. The electrical activity in the axonal plexus of these neurons is thought to propagate antidromically into cell somata and dendrites, and interact with synaptic input to modify those synapses or to regulate orthodromic output [16].

The present study was undertaken to search for evidence of the presence of gap junctions along axons, specifically within short distances of their emergence from neuronal somata where they have been predicted to occur. As a convenient marker for this axonal region, we used immunofluorescence labelling for ankyrinG, which is a scaffolding protein highly concentrated along AISs that span 20 to 70 µm distally from the axon hillock [17]. Because Cx36 is highly expressed in neurons and is a robust marker for their gap junctions [6], we sought to determine in several CNS regions whether Cx36 is localized at AISs.

### Materials and methods

#### *Animals and antibodies*

All animals in this study were obtained and used in concordance with approved protocols put in place by the Central Animal Care Committee of the University of Manitoba. A total of 18 adult male CD1 mice and 8 C57BL/6 mice weighing between 25 to 35 grams were used in this study. A total of 6 male mice at 15 days of age were used. No discernible qualitative differences in the results were found between the two strains. The mice were obtained from breeding colonies maintained at the University of Manitoba. Immunofluorescence labelling in CNS tissues was performed using six different antibodies in double or triple labelling combinations. A mouse monoclonal anti-Cx36 antibody (Cat. No. 39-4200) was obtained from ThermoFisher Scientific (Waltham, MA, USA) and used at a concentration of 3 µg/ml for incubation with tissue sections. This antibody was previously shown to detect Cx36 by western blotting [18], and to produce intense

immunofluorescence labelling for Cx36 in the form of Cx36-puncta in various brain and spinal cord regions, which were absent in Cx36 null mice [19-22]. Other antibodies included: a polyclonal chicken anti-ankyrinG antibody (Cat. No. CPCA-ANK3) acquired from EnCor Biotechnology Inc (Gainesville, FL, USA) and used at a dilution of 1:1000; a goat polyclonal anti-ankyrinG antibody (Cat. No. sc-31778) obtained from Santa Cruz Biotechnology Inc. (Santa Cruz, CA, USA) and used at a dilution of 1:1000; a chicken polyclonal anti-peripherin antibody (Cat. No. AB9282) obtained from Millipore EMD (Burlington, MA, USA) and used at a dilution of 1:500; a rabbit anti-glutamate decarboxylase (GAD) antibody prepared as previously described [23] (generously provided by Dr. E. Roberts) and used at 1:1000; and a rabbit polyclonal anti-ZO-1 antibody (Cat. No. 61-7300) obtained from ThermoFisher Scientific and used at a concentration of 4 µg/ml.

#### *Tissue preparation and immunofluorescence labelling*

Animals were anesthetized by an intraperitoneal injection of equithesin (3 ml/kg) and immediately perfused transcardially with 6 ml of cold (4°C) prefix solution composed of 50 mM sodium phosphate buffer, pH 7.4, 0.9% NaCl, 0.1% sodium nitrite and 1 unit/ml heparin. Animals were then perfused with 50 ml of a fixative solution consisting of 0.16 M sodium phosphate, pH 7.1, 0.2% picric acid and either 1% or 2% formaldehyde (Electron Microscopy Sciences, Hatfield, PA, USA). Following perfusion with fixative, animals were perfused with 10 ml of 25 mM sodium phosphate buffer, pH 7.4, containing 10% sucrose. The spinal cord and brain were dissected and transferred to cryoprotectant solution consisting of 25 mM sodium phosphate buffer, pH 7.4, 10% sucrose and 0.04% sodium azide, and stored at 4°C for 2 days. The tissue was then flash frozen, cryosectioned at 15 µm in the transverse plane, and sections were collected on gelatinized slides and stored at -30°C.

For immunofluorescence processing, slide-mounted sections were thawed to room temperature and rinsed for 20 min in 50 mM Tris-HCl buffer, pH 7.4, containing 1.5% sodium chloride (TBS) and 0.3% Triton X-100 (TBST). Sections were incubated at 4°C for 12 to 18 h simultaneously with two or three different pri-

mary antibodies diluted in TBST containing 10% normal donkey serum. After incubation with primary antibodies, sections on slides were washed three times for 20 min in TBST and then incubated with appropriate combinations of secondary antibodies, all produced in donkey (Jackson ImmunoResearch), including Cy5-conjugated anti-chicken and anti-rabbit diluted 1:600, Cy3-conjugated anti-mouse diluted 1:600 and AlexaFluor 488-conjugated anti-chicken and anti-goat diluted 1:1000. Sections were incubated with secondary antibodies for 1.5 h at room temperature, then washed for 20 min in TBST and then washed twice for 20 min in 50 mM Tris-HCl buffer, pH 7.4, and subsequently coverslipped with Fluoromount G anti-fade medium (SouthernBiotech, Birmingham, USA). The slides were air dried for 1 h before placing them at -20°C for long term storage.

### *Immunofluorescence microscopy*

Tissue sections were examined and photographed by wide-field microscopy using a Zeiss Z2 Axiovision Imager microscope, a Zeiss 710 confocal laser scanning microscope and at high resolution using confocal Zeiss Elyra-SIM microscope configured for structured illumination microscopy (SIM). Images were collected as czi files using Zeiss Zen Blue and Zen Black software (Carl Zeiss Canada, Toronto, Canada). Wide-field and confocal images were collected either as single-scans or z-stacks ranging from 10 to 19 scans thereby capturing a thickness of approximately 4 to 8 µm of tissue at z scanning intervals of typically ~0.4 µm using a ×40 objective lens. Final images were assembled using CorelDraw Graphics (Corel Corp., Ottawa, Canada). Images with Cy5 immunolabelling were pseudocoloured either blue or cyan.

Several procedures were used as search strategies for localization of Cx36-puncta on AISs. In each CNS area examined, numerous randomly selected fields measuring 100×100 µm were photographed. Each z-stack image was first viewed as a maximum intensity projection to obtain an overview of possible AIS/Cx36-puncta association. If overlap of labels for ankyrinG and Cx36 was seen, which was often the case in areas with moderate to high densities of Cx36-puncta, we next examined z-stack images by 3D rendering in transparency mode, with image rotation in x and y axis to

exclude cases where labels for AISs and Cx36 overlapped, but were separated in the z axis, and to confirm cases where labels were found that overlapped in the x and y axes and were not separated in the z axis. Single consecutive scan images within the compiled z-stack were then visually scrutinized at high digital image magnification to further confirm qualitatively the association of labels for AIS and Cx36-puncta in all three axes. Using Zeiss Zen software tools and raw (*i.e.*, unadjusted for displayed intensity) single scan images, the immunofluorescence intensity profiles at selected sites of AIS/Cx36-puncta co-localization were captured at high digital magnification.

## Results

### *Cx36-puncta at AISs in spinal cord*

Our initial observations of Cx36 association with AISs were conducted using mouse lumbar spinal cord at postnatal day (PD) 10, where we found examples of Cx36 localization at the AIS of motoneurons in lamina IX [12]. To determine if this localization was a developmentally transient phenomenon, we first examined the prevalence of Cx36/AIS association in lumbar segments from mice at PD 15, which is roughly when expression of Cx36 peaks in the CNS followed by a gradual decline [24]. In a first set of sections, ankyrinG was used as a robust marker for AISs [25, 26] and peripherin - an intermediate filament protein - as a marker for motoneurons [27, 28]. A second set of sections at PD 15 was taken for labelling of Cx36, ankyrinG and GAD to ascertain possible association of Cx36 with GABAergic terminals contacting AISs. In each set of sections, confocal images were collected in five randomly selected fields measuring 100×100 µm in each of laminae III to X, excluding laminae I and II that had very low labelling for Cx36. In the first set of sections, 77 cases were found where labelling for Cx36 in the form of Cx36-puncta was localized to ankyrinG+ (positive) AISs, with an average incidence of  $1.9 \pm 0.2$  Cx36-puncta/AIS co-localization per field. In the second set of sections where 68 Cx36-puncta/AIS co-localization cases were found, there was negligible association of GAD+ nerve terminals with Cx36 localized at AISs. Similar analyses of Cx36-puncta associated with AISs in adult mouse lumbar spinal cord gave an incidence of  $1.3 \pm 0.8$  Cx36-puncta/AIS co-localization in a total of 40 fields exam-

## Connexin36 at axon initial segments

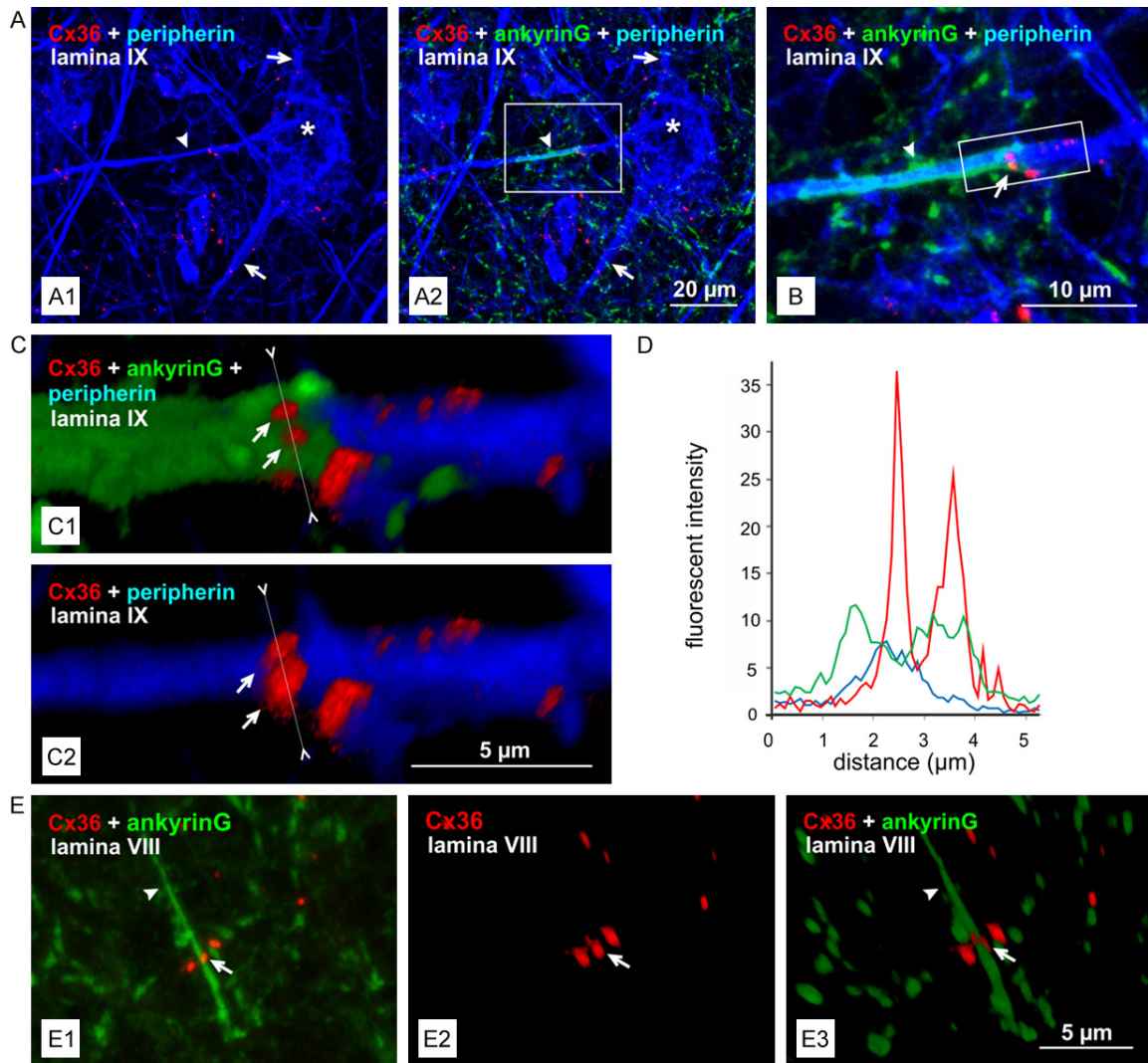


**Figure 1.** (A) Low magnification immunofluorescence image in lamina IX of PD 15 mouse lumbar spinal cord, showing Cx36-puncta distributed in the vicinity of a peripherin + motoneuron soma (A1, A2, asterisk) extending a peripherin+ axon (A1, A2, arrowhead) and initial dendrites (A1, A2, arrows), and showing in the same field the ankyrinG+ motoneuron AIS (A2, arrowhead). (B) Magnification of the boxed area in (A2), showing Cx36-puncta (arrow) associated with the ankyrinG+ AIS (arrowhead). (C) Magnification of the boxed area in (B) shown as 3D-rendered images with overlay of labelling for Cx36 (C1, arrows), ankyrinG and peripherin (C1) and in the same image labelling for only Cx36 and peripherin (C2). (D) IFIP of labelling for Cx36, ankyrinG and peripherin along the white line segment bracketed by arrowheads in (C1), showing correspondence of peak intensities for each of the three colors plotted. (E) Example of Cx36-punctum (arrow) associated with an ankyrinG+ AIS (arrowhead) in lamina VIII. The images in (E2 and E3) are 3D-rendered versions of maximum intensity projections shown in (E1).

ined. This reduced Cx36/AIS association in adult mice parallels the overall decrease in Cx36 expression in adult vs. neonatal animals [29], although differences in cytoarchitectural features of the spinal cord at the two ages precluded validity of statistical comparison. Because labelling for ankyrinG in spinal cord grey matter was very dense, with only short fragments (100-200) of AISs observed per field, no attempt was made to count total num-

bers of these per field, thus precluding estimates of the proportion of AISs harbouring Cx36-puncta.

Data on relationships between Cx36-puncta and AISs in mouse spinal cord at PD 15 is shown in **Figures 1** and **2**. An example of Cx36-puncta localized to an ankyrinG+ AIS of a peripherin+ axon emanating from a motoneuron soma in lamina IX is shown in **Figure 1A-C**.

## Connexin36 at axon initial segments

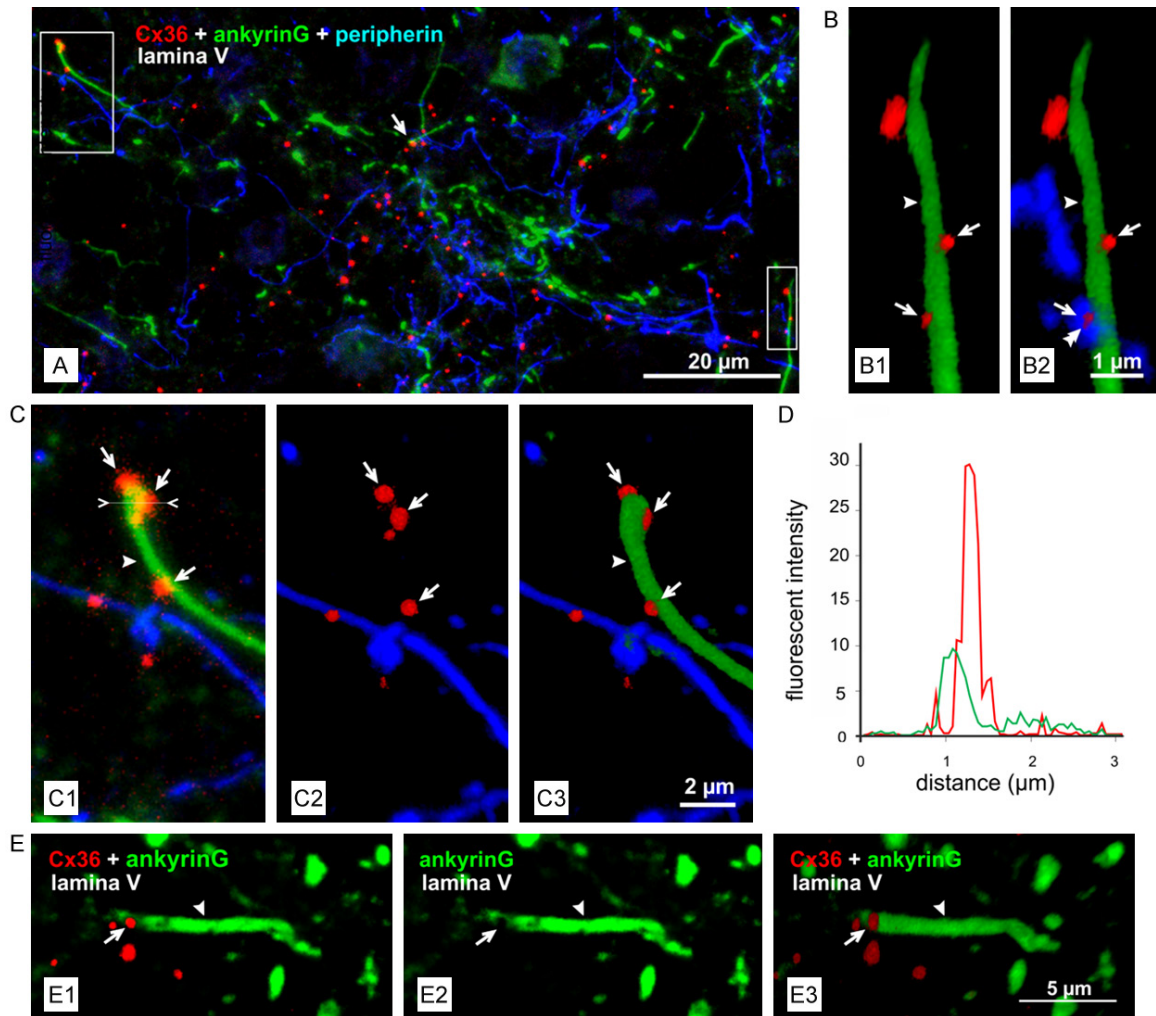


**Figure 2.** (A) Low magnification immunofluorescence image in an area of PD 15 mouse lumbar spinal cord lamina V with overlay of labelling for Cx36, ankyrinG and peripherin, showing three examples of Cx36-puncta associated with ankyrinG+ AIS (arrow and two boxed areas). (B) Magnification of the boxed area in the lower right in (A) with red/green overlay (B1) and triple color overlay (B2) of 3D-rendered images, showing two Cx36-puncta (arrows) localized to an AIS (arrowhead) (B1), where one of the Cx36-puncta appears in an area that is also peripherin+ (B2, double arrowhead). (C) Magnification of the boxed area in the upper left in (A), shown as maximum intensity projection (C1) and 3D-rendered images (C2, C3), showing three Cx36-puncta (C2, arrows) associated with labelling for ankyrinG (C3, arrowhead) at the AIS (C3, arrowhead). None of the three puncta are associated with labelling for peripherin. (D) IFIP of labelling for Cx36 and ankyrinG along the white line segment bracketed by arrowheads in (C1), showing substantial overlap of peak labelling intensities for Cx36 and ankyrinG. (E) Example of Cx36-punctum (arrow) associated with an ankyrinG+ AIS (arrowhead) in lamina V, where the Cx36-punctum in the red/green overlay in the maximum intensity projection and 3D-rendered images of (E1 and E3), respectively, is located in a region of AIS largely devoid of labelling for ankyrinG, as shown in (E2) with the red channel of label for Cx36 turned off.

At all other locations in the mammalian CNS, Cx36 was detected exclusively in the form of Cx36-puncta that are widely accepted to reflect the localization of neuronal gap junctions [6]. Labelling of Cx36 at all AISs examined had a similar punctate appearance, and the AIS in **Figure 1B** harboured two Cx36-puncta. As evident by comparison of 3D-rendered images in

**Figure 1C1** vs. **Figure 1C2**, these puncta were partially obscured by immunolabelling of ankyrinG, which is localized to the inner surface of the AIS. Among the procedures used to confirm AIS/Cx36-puncta association was the immunofluorescence intensity profile (IFIP) tool for ankyrinG and Cx36 labels at sites of their colocalization in consecutive through-focus imag-

es. An IFIP of labelling for Cx36, ankyrinG and peripherin taken through a line perpendicular to the axis of the AIS is shown in **Figure 1D**. Peak fluorescence intensity for labels of Cx36 and ankyrinG overlap, while intensity for peripherin falls off at the edges, possibly due to the more centralized localization of peripherin-based intermediate filaments along the axon. Detection of Cx36 at an AIS in laminae VIII is shown in **Figure 1E** as maximum intensity projection and 3D-rendered images, where Cx36-puncta were seen embedded in labelling for ankyrinG (**Figures 1E2** and **1E3**). The relative density of labelling for the various markers used and an instance of three AISs displaying Cx36-puncta, including multiple puncta, is shown in a field of lamina V (**Figure 2A**). The boxed areas in **Figure 2A** are shown as 3D rendered (**Figure 2B, 2C2** and **2C3**) and maximum intensity projection images (**Figure 2C1**). A comparison of Cx36-puncta associated with the AIS in **Figure 2C2** and **2C3** shows that these puncta protrude somewhat from the AIS, such that they were larger with the green channel turned off, indicating that the bulk of the puncta were embedded in the AIS. In **Figure 2B**, one of the two Cx36-puncta is co-localized with a peripherin-positive element that likely belongs to a primary afferent axon terminating in the dorsal horn. An IFIP taken through one of the AIS-associated Cx36-puncta (**Figure 2C1**) again showed partial overlap of peak intensity of labelling for Cx36 and ankyrinG (**Figure 2D**). Labelling for ankyrinG was sometimes reduced in intensity in the area occupied by a Cx36-punctum (**Figure 2E**), suggesting displacement of structural ankyrinG at locations of these puncta in axonal plasma membranes.

### *Cx36 at AISs in the inferior olive*

We next examined Cx36/AIS association in adult mouse inferior olivary nucleus, which is among brain regions with the greatest expression levels of Cx36 [2]. In contrast to AIS patterns in spinal cord, long ankyrinG+ AISs were prominent in the inferior olive and some of these displayed Cx36-puncta along their length (**Figure 3A**). In 21 fields measuring 100×100 µm, a total of 38 Cx36-puncta were found localized to AISs, with typically one punctum per AIS, and an average of ~2 AISs per field displaying Cx36-puncta. Cx36-puncta associated with AISs had an average diameter of  $0.50 \pm 0.02$  µm (mean  $\pm$  s.e.m.,  $n = 16$ ), which was not dif-

ferent from the average diameter ( $0.51 \pm 0.19$  µm,  $n = 16$ ) of those in the vicinity of AISs. Counts of AISs that were 10 µm or longer in the 21 fields gave an average of  $25.9 \pm 2.7$  (mean  $\pm$  s.e.m.) AISs per field, from which it was calculated that ~7% of AISs per field showed association with Cx36-puncta. In rare instances, Cx36-puncta were seen associated with two AISs having close proximity (**Figure 3B1**), with Cx36-puncta occurring at possible axonal apposition, though this was not possible to discern. In addition to labelling for Cx36 and ankyrinG, all sections of the inferior olive were simultaneously labelled for GAD to determine possible association of Cx36-puncta with GABAergic terminals that synapse on AISs [26]. Cx36-puncta localized to AISs showed negligible association with GAD-positive terminals (**Figure 3B**). Image rotation (**Figure 3C**) and IFIP (**Figure 3D, 3E**) confirmed Cx36-puncta localization at AISs in the inferior olive.

We next sought to determine whether Cx36-puncta localized to AISs exhibited a molecular signature that is characteristic of functional Cx36-containing gap junctions found at other neuronal subcellular compartments. A recurring feature of many connexins is their molecular interaction with the scaffolding protein ZO-1, specifically at gap junctions where this protein appears to contribute to junctional integrity, assembly and turnover [30]. This is also true for electrical synapses formed by gap junctions between neurons, where we have shown that ZO-1 is a constituent of nearly all, if not all, Cx36-containing gap junctions in various CNS areas [4, 5, 31]. Taking the inferior olive as a representative region, triple immunofluorescence labelling indicated that ZO-1 was exactly localized to Cx36-puncta at sites where these puncta were associated with AISs (**Figure 3F**). This was observed in twelve inferior olive fields examined, where a total of 24 Cx36-puncta associated with AISs were all found to have near exact overlap of labelling for ZO-1. Using the image in **Figure 3F**, IFIP confirmed the overlap of peak fluorescent intensities of the labels for Cx36, ZO-1 and ankyrinG (**Figure 3G**). This result is in keeping with the possibility that Cx36 is organized into gap junction plaques at AISs, which appears to be promoted by ZO-1, as elsewhere in the CNS.

To further confirm Cx36-puncta/AIS co-localization, we examined this in the inferior olive by

## Connexin36 at axon initial segments

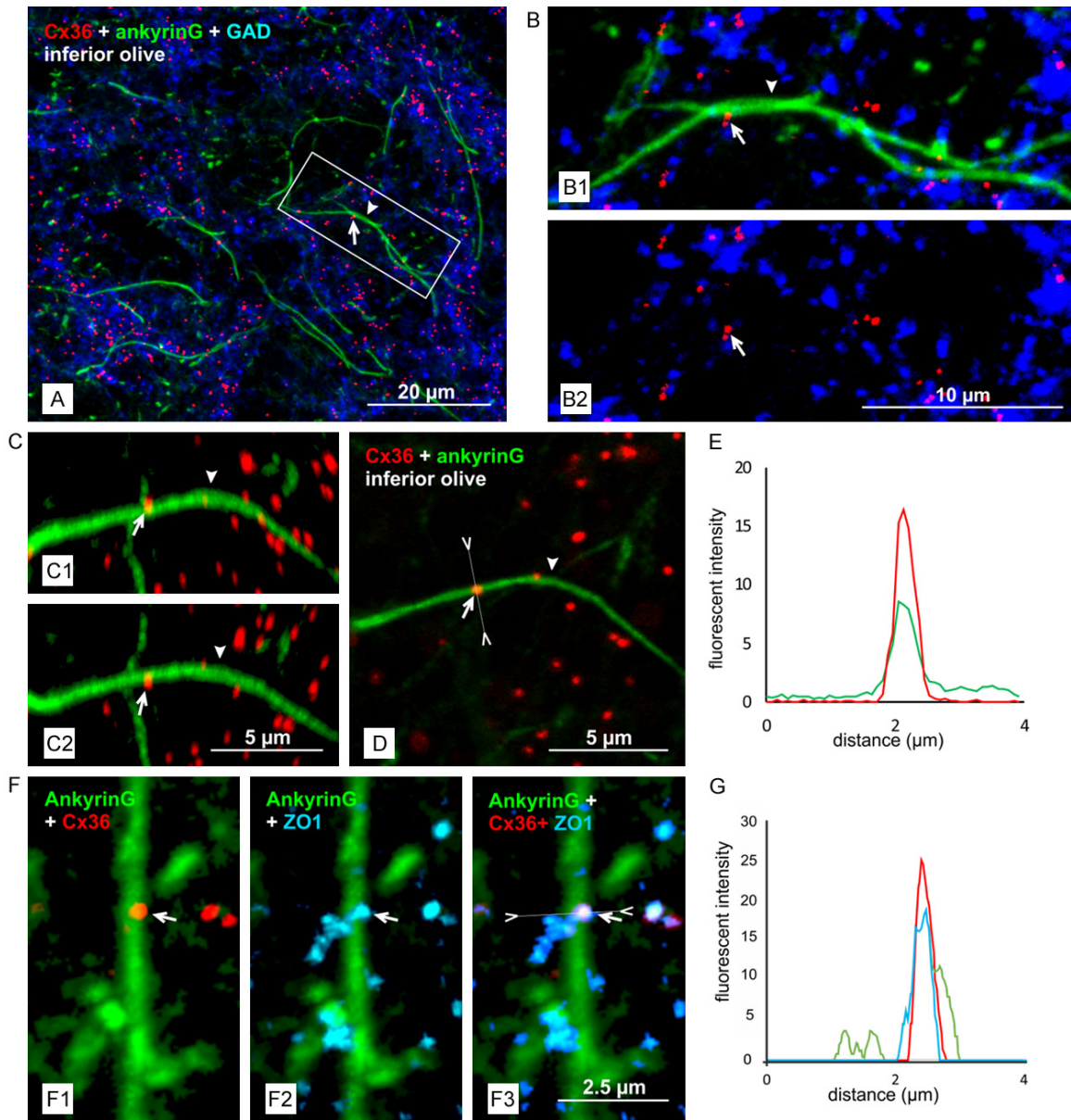


**Figure 3.** (A) Low magnification immunofluorescence overlay image showing the appearance of labelling for Cx36, ankyrinG and GAD in the inferior olive of adult mouse. (B) Magnification of the boxed area in (A), showing localization of a Cx36-punctum (B1, arrow) at a point of close proximity between one AIS and another (B1, arrowhead). The AIS-associated Cx36-punctum lacks co-localization with labelling for GAD (B2, arrow). (C) A z-stack image of an AIS-associated Cx36-punctum (arrow) on an AIS (arrowhead) in the inferior olive, where image rotation by 90° in the x-plane (C1 vs. C2) shows persistent co-localization of the punctum with the AIS. (D, E) IFIP taken along the white line segment through labelling at a Cx36-punctum (D, arrow) localized on an ankyrinG+ AIS (D, arrowhead), showing correspondence of peak labelling intensity for Cx36 at the point of its association with the AIS (E). (F) Triple immunofluorescence showing an AIS-associated Cx36-punctum (F1, arrow) labelled for ZO-1 (F2, arrow), as seen in triple overlay (F3, arrow). (G) IFIP of the AIS-associated punctum in (F3), showing correspondence of peak intensity labelling for ankyrinG, Cx36 and ZO-1.

structured illumination microscopy (SIM), which provides higher resolution than afforded by standard confocal imaging. Results obtained were similar to those described above; six

images were obtained where Cx36-puncta were found to be entirely embedded within or at the edge of ankyrinG+ AISs and where IFIP showed correspondence of peak intensities

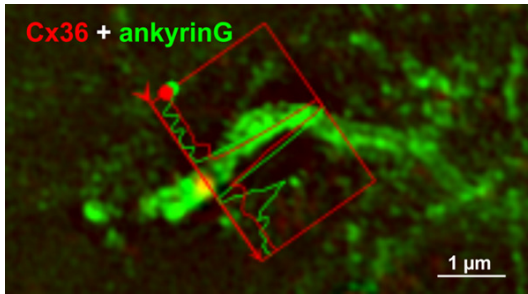


**Figure 4.** Superresolution image taken by SIM showing a Cx36-punctum localized to an ankyrin+ AIS in the inferior olive of adult mouse. The punctum appears yellow in red/green overlay. IFIP along the red line bracketed by arrowheads and intersecting the Cx36-punctum on the AIS shows correspondence of peak intensities for the red and green labels.

(**Figure 4**). Localization of Cx36-puncta at AISs was additionally established by through-focus examination and image rotation.

### *Cx36 at AISs in the cerebral cortex*

Another region examined was the parietal cerebral cortex in adult mouse, where vertically oriented AISs ranging from 15 to 30 µm in length and from 0.5 to 1.0 µm in diameter were prominent (**Figure 5A1**) and could occasionally be followed to their origin from large neuronal somata (e.g., principal cells) in layers IV/V, and to large neurons in layer III. It was these that were taken for examination and quantification of Cx36-puncta/AIS association among the Cx36-puncta found in these layers (**Figure 5A2, 5A3**). Cx36-puncta were found localized to AISs in the various cortical layers. An example of Cx36/AIS co-localization in consecutive through-focus images in cortical layer IV/V is shown in **Figure 5B**, together with IFIP of labels for ankyrinG and Cx36 at a site of their co-localization at each step of through focus (**Figure 5C**). The IFIP for each image indicates consistent overlap of labelling for ankyrinG and Cx36 at each level of focus. Correspondence of the peak intensity for the two labels was substantial but variable, which is consistent with observations that Cx36-puncta often protrude slightly from the axis cylinder of the AIS (e.g., **Figure 2**). The image in **Figure 5B** is shown as a maximum intensity projection with 3D image rotation in [Supplementary Movie 1](#), confirming Cx36/AIS association at all angles of rotation.

### *Lack of Cx36 at AISs in the hippocampus*

In the hippocampus, AISs extending from principal cells in the CA1, CA2 and CA3 regions were prominent and were localized superficial to these cells in the stratum oriens, as shown in the CA1 region (**Figure 6A1**). Despite robust punctate labelling for Cx36 in many hippocampal regions, areas where AISs of pyramidal cells were most concentrated, as well as areas extending somewhat dorsal to the AIS plexus, were nearly entirely devoid of Cx36-puncta (**Figure 6A2**), thus precluding their AIS association, and the few Cx36-puncta that were seen in the vicinity of AISs lacked association with these ankyrin+ structures (**Figure 6B**).

## Discussion

Among subcellular neuronal compartments, the AIS is a privileged site because it plays a dominant role in action potential initiation and contributes to a variety of other processes, including maintenance of neuronal polarity, provision of a protein diffusion barrier and regulation of intracellular trafficking, for which reasons it has been a topic of intense investigation for the past several decades [17, 26, 32, 33]. To the list of activities and molecular features that distinguishes the AIS, we now add the targeting of Cx36 to this region of the axon. Localization of Cx36 at AISs is supported by our use of standard and super resolution imaging, IFIP, 3D image rotation and through-focus analyses of z-stack images, all of which showed Cx36-embedded within AISs, and by the co-localization of Cx36-puncta and a gap junction-associated protein (i.e., ZO-1) at sites of Cx36-puncta/AIS association. Our findings raise a number of questions concerning the long predicted existence of axo-axonic gap junctions.

### *Structural composition of Cx36 at AISs*

The first question concerns the structure in which Cx36 is configured at AISs. By immunofluorescence labelling, Cx36 detected along AISs had the same punctate appearance and a comparable size of Cx36-puncta as found in many other CNS regions, where it has been established by a variety of ultrastructural and molecular criteria that these puncta represent sites of neuronal gap junctions [5, 6, 34, 35]. The Cx36-puncta localized to AISs were often

## Connexin36 at axon initial segments

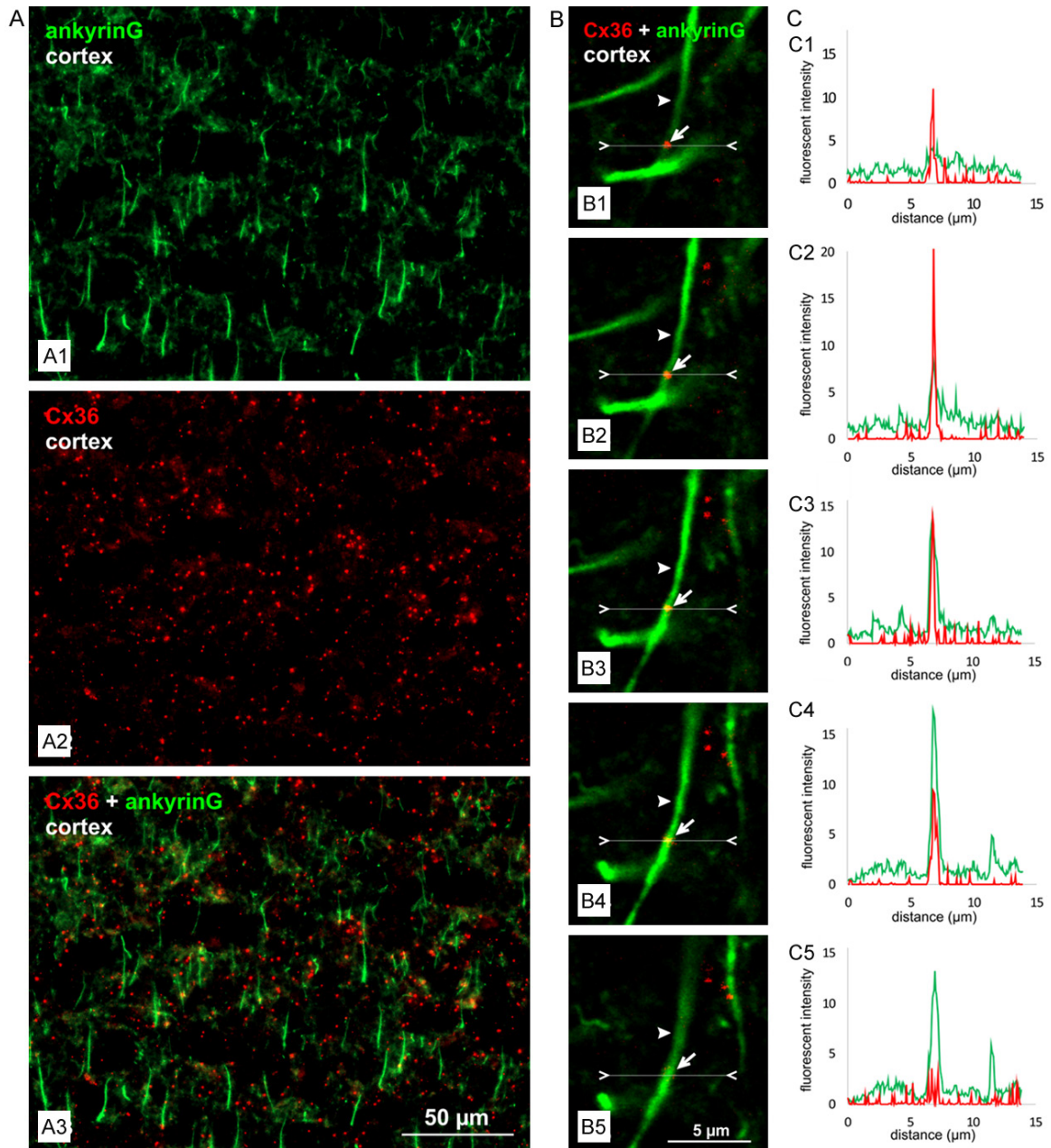


**Figure 5.** (A) Low magnification immunofluorescence images showing the distribution and density of labelling for ankyrinG (A1) and Cx36 (A2) in layers IV/V of parietal cerebral cortex of adult mouse, with some Cx36-puncta in close proximity or overlapping with ankyrinG+ AIS, as seen in overlay (A3). (B) A set of five consecutive through-focus images taken from a z-stack series encompassing the upper (B1) and lower (B5) limits of co-localization between a Cx36-punctum (arrow) and an ankyrinG+ AIS (arrowhead) in adult mouse cerebral cortex. (C) IFIP of labelling for Cx36 and ankyrinG along the white line segments bracketed by arrowheads in (B) and drawn through the Cx36-punctum localized to the AIS. The profiles represent data taken from corresponding images to their left, and show matching patterns of peak intensities of labelling for Cx36 and ankyrinG.

seen protruding slightly out from the ankyrinG+ region of the axon, as further confirmed by visualization of these puncta with or without the green channel on (*i.e.*, labelling for ankyrinG), where the Cx36-puncta invariably had a larger

portion extending into the axon and contiguous with the protruding portion. This was also evident from some of the IFIP, suggesting the presence of an unseen coupling partner. The AIS-associated Cx36-puncta examined in the infe-

## Connexin36 at axon initial segments

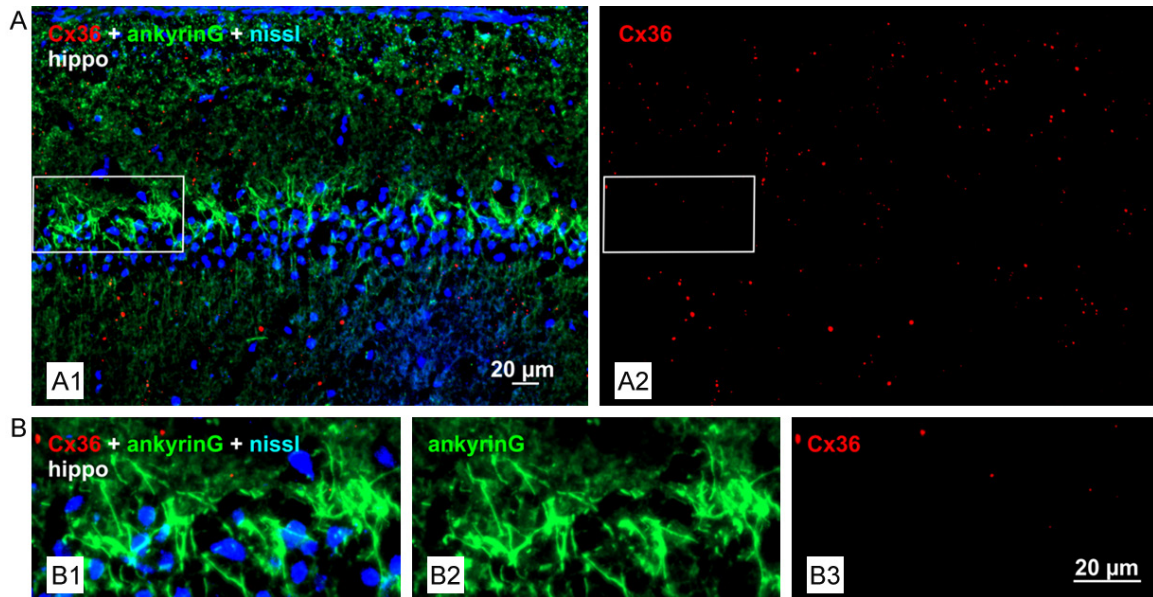


**Figure 6.** (A) Low magnification immunofluorescence image of the CA1 region of the hippocampus in adult mouse showing labelling of Cx36 and ankyrinG in a fluorescence nissl stained section. Pyramidal cells (blue) display ankyrinG+ AISs (green) extending dorsally from the pyramidal cell layer (A1), where labelling for Cx36 in the same field is very sparse (A2). (B) Higher magnification of the boxed area in (A), showing triple fluorescence overlay (B1), with very few Cx36-puncta (B3) in a field containing many AISs (B2).

rior olive and spinal cord shared a feature characteristic of functional Cx36-containing neuronal gap junctions elsewhere in the CNS, namely their precise overlap of labelling for ZO-1. These points support the possibility that Cx36-puncta at AISs, as elsewhere in the CNS, correspond to bona fide gap junctions.

It may be considered that immunocytochemically-detected Cx36-puncta along AIS represents Cx36 undergoing axonal transport, but the above points largely exclude this possibility; Cx36-puncta appeared to traverse the plasma membrane, whereas axonal transport would occur intracellularly, via membrane bounded organelles, which remain undetected by immunofluorescence labelling of Cx36 [6].

### *AIS gap junction coupling partners*

If Cx36-puncta at AISs indeed form typical intercellular communication channels, then a second question concerns the identity of the AIS coupling partner. One possible class of candidates are nerve terminals contacting AISs, forming mixed synapses such as we have described in a number of mammalian CNS regions [8, 20, 21, 36]. So far, however, we have found only excitatory glutamatergic mixed syn-

apses in those regions, and to our knowledge there is no evidence for excitatory terminal contacts on AISs. Alternatively, terminals that release gamma-aminobutyric acid (GABA) are known to form synapses with AISs in some brain regions [17], and widespread subclasses of GABAergic neurons are known to express Cx36 [37, 38]. However, our results revealed that Cx36-puncta on AISs lacked co-localization with the GABAergic terminal marker GAD. This is consistent with findings in some of the CNS areas we examined, such as the inferior olive, where AISs have few if any synaptic contacts [39]. Dendro-axonic contacts at Cx36-puncta/AIS associations remain a possibility, but there appears to be little precedent for this structural arrangement.

Of particular interest, as elaborated in the Introduction, is the possible mediation of axo-axonic electrical coupling by gap junctions localized to axons. The existence of such axo-axonic coupling would be expected to yield situations where AISs intersect at points where they harbour Cx36-puncta. In a variety of other systems, Cx36-puncta can readily be visualized at points of contact between appropriately labelled gap-junctionally coupled neuronal elements [6, 40]. However, in the many

## Connexin36 at axon initial segments

images examined here, we found only a few instances of Cx36-puncta that may be localized at AIS intersections. It should be noted though that ankyrinG+ AISs ranging from 20-70  $\mu\text{m}$  may not represent the full extent along which axo-axonic coupling could potentially occur over the  $\sim 150$   $\mu\text{m}$  of initial axons where coupling has been predicted (see Introduction), particularly since axons may remain unmyelinated for some distance beyond the AIS in some brain areas [41]. Thus, it remains to be determined whether Cx36-puncta on AISs occur at contacts between ankyrinG+ and ankyrinG-negative axonal segments.

### *Incidence of Cx36-puncta at AIS*

Though not exceptionally rare, AISs displaying Cx36-puncta had a low frequency of occurrence and typically displayed a single punctum along their length. Thus, a final question is whether this low incidence could have a functional impact if these puncta do in fact correspond to axo-axonic electrical synapses. In this regard, factors surrounding neuronal network activity such as high frequency oscillations that have been considered to be influenced by these putative synapses have been the subject of extensive computer modelling. A key point predicted by this modelling is that a very low density of axonal gap junctions can lead to network oscillations, provided that each axon couples to more than one other axon and provided that action potentials can cross from axon to axon via electrical synapses. For example, it was found that an average density of only 1.6 gap junctions/axon could lead to very fast oscillations ( $>100$  Hz) [11, 42-45]. Axo-axonal mediated spiking is difficult to establish in mammalian systems, but its occurrence is supported indirectly by observations that somatically induced spikes can evoke somatic spikes in a coupled cell in systems where dendritic or somatic gap junctions have not been found and where coupling may therefore be mediated by axonal gap junctions [14, 15, 46]. Notwithstanding these points, a possible role of Cx36 in axo-axonic synapse formation at AISs is somewhat diminished in the hippocampus which lacked Cx36-puncta at or in the vicinity of AISs of principal cells, consistent with observations that *in vivo*  $\sim 200$  Hz oscillations survive knock-out of Cx36 [47], but we cannot exclude the involve-

ment of another connexin, as discussed elsewhere [12].

### *Cx36-puncta at AIS in hindbrain and spinal cord*

Unlike cortical structures, there has been less consideration of possible relationships between axo-axonal interactions and high frequency oscillations in lower CNS centers. Our finding of Cx36-puncta localized to AISs of inferior olivary neurons was therefore somewhat unexpected. The functional role of these puncta and whether they are indicative of axonal gap junctions coupled to an as yet unidentified partner remains to be investigated. This notwithstanding, our findings of Cx36-puncta localized to AIS of olivary neurons may be considered in relation to observations of high frequency spike bursts initiated within the axons of these neurons, with the generation of these dependent on the presence of intact axons extending at least 100  $\mu\text{m}$  beyond the neuronal soma [48], raising the possibility of burst generation by axo-axonal interactions. With respect to Cx36-puncta at AISs in spinal cord, we note that neurogenic muscle cramps are associated with high-frequency discharges in electromyographic recordings, suggesting that spinal motoneurons and/or their axons are collectively firing at high frequencies, mediated perhaps via "ephaptic" interactions as has been suggested [49], or alternatively by transmission via electrical synapses, which is a possibility raised by our finding of Cx36-puncta association with motoneuronal axons.

### **Acknowledgements**

This work was supported by grants from the Canadian Institutes of Health Research and the Canadian Natural Sciences and Engineering Research Council to J. I. Nagy and the IBM Corporation Exploratory Research Councils to R. D. Traub.

### **Disclosure of conflict of interest**

None.

**Address correspondence to:** Dr. James I Nagy, Department of Physiology and Pathophysiology, Max Rady College of Medicine, University of Manitoba, 745 Bannatyne Ave, Winnipeg, Manitoba R3E 0J9, Canada. Tel: (204) 789-3767; Fax: (204) 789-3934; E-mail: James.Nagy@umanitoba.ca

### References

- [1] Pereda AE. Electrical synapses and their functional interactions with chemical synapses. *Nat Rev Neurosci* 2014; 15: 250-263.
- [2] Connors BW. Develop synchrony and so much more: diverse roles for electrical synapses in neural circuits. *Dev Neurobiol* 2017; 77: 610-624.
- [3] Alcami P and Pereda AE. Beyond plasticity: the dynamic impact of electrical synapses on neural circuits. *Nat Rev Neurosci* 2019; 20: 253-271.
- [4] Li X, Olson C, Lu S, Kamasawa N, Yasumura T, Rash JE and Nagy JI. Neuronal connexin36 association with zonula occludens-1 protein (ZO-1) in mouse brain and interaction with the first PDZ domain of ZO-1. *Eur J Neurosci* 2004; 19: 2132-2146.
- [5] Nagy JI and Lynn BD. Structural and intermolecular associations between connexin36 and protein components of the adherens junction-neuronal gap junction complex. *Neuroscience* 2018; 384: 241-261.
- [6] Nagy JI, Pereda AE and Rash JE. Electrical synapses in mammalian CNS: past eras, present focus and future directions. *Biochim Biophys Acta* 2018; 1860: 102-123.
- [7] Pereda AE and Bennett MVL. Electrical synapses in fishes: their relevance to synaptic transmission. In: J. Jing, editor. *Network Functions and Plasticity*. Academic Press; London: 2017. pp. 161-181.
- [8] Nagy JI, Pereda AE and Rash JE. On the occurrence and enigmatic functions of mixed (chemical plus electrical) synapses in the mammalian CNS. *Neurosci Lett* 2019; 695: 53-64.
- [9] Bennett MV, Nakajima Y and Pappas GD. Physiology and ultrastructure of electrotonic junctions. I. Supramedullary neurons. *J Neurophysiol* 1967; 30: 161-179.
- [10] Yasargil GM and Sandri C. Topography and ultrastructure of commissural interneurons that may establish reciprocal inhibitory connections of the Mauthner axons in the spinal cord of the tench, *Tinca tinca* L. *J Neurocytol* 1990; 19: 111-126.
- [11] Traub RD and Whittington MA. *Cortical oscillations in health and disease*. Oxford University Press; New York: 2010.
- [12] Traub RD, Whittington MA, Maier N, Schmitz D and Nagy JI. Could electrical coupling contribute to the formation of cell assemblies? *Rev Neurosci* 2020; 28: 121-141.
- [13] Traub RD, Draguhn A, Whittington MA, Baldeweg T, Bibbig A, Buhl EH and Schmitz D. Axonal gap junctions between principal neurons: a novel source of network oscillations, and perhaps epileptogenesis. *Rev Neurosci* 2002; 13: 1-30.
- [14] Schmitz D, Schuchmann S, Fisahan A, Draguhn A, Buhl EH, Petrasch-Parwez E, Dermietzel R, Heinemann U and Traub RD. Axo-axonal coupling: a novel mechanism for ultrafast neuronal communication. *Neuron* 2001; 31: 831-840.
- [15] Wang Y, Barakat A and Zhou H. Electrotonic coupling between pyramidal neurons in the neocortex. *PLoS One* 2010; 5: 1-9.
- [16] Bukalo O, Campanac E, Hoffman DA and Fields RD. Synaptic plasticity by antidromic firing during hippocampal network oscillations. *Proc Natl Acad Sci U S A* 2013; 110: 5175-5180.
- [17] Leterrier C. The axon initial segment, 50 years later: a nexus for neuronal organization and function. *Curr Top Membr* 2016; 77: 185-233.
- [18] Li X, Lynn BD and Nagy JI. The effector and scaffolding proteins AF6 and MUPP1 interact with connexin36 and localize at gap junctions that form electrical synapses in rodent brain. *Eur J Neurosci* 2012; 35: 166-181.
- [19] Curti S, Hoge G, Nagy JI and Pereda AE. Synergy between electrical coupling and membrane properties promotes strong synchronization of neurons of the mesencephalic trigeminal nucleus. *J Neurosci* 2012; 32: 4341-4359.
- [20] Bautista W and Nagy JI. Connexin36 in gap junctions forming electrical synapses between motoneurons in sexually dimorphic motor nuclei in spinal cord of rat and mouse. *Eur J Neurosci* 2014; 39: 771-787.
- [21] Bautista W, McCrear DA and Nagy JI. Connexin36 identified at morphologically mixed chemical/electrical synapses on trigeminal motoneurons and at primary afferent terminals on spinal cord neurons in adult mouse and rat. *Neuroscience* 2014; 263: 159-180.
- [22] Rubio ME and Nagy J. Connexin36 expression in major centers of the auditory system in the CNS of mouse and rat: evidence for neurons forming purely electrical synapses and morphologically mixed synapses. *Neuroscience* 2015; 303: 604-629.
- [23] Wu JY, Matsuda T and Roberts E. Purification and characterization of glutamate decarboxylase from mouse brain. *J Biol Chem* 1973; 248: 3029-3034.
- [24] Belousov AB and Fontes JD. Neuronal gap junctions: making and breaking connections during development and injury. *Trends Neurosci* 2013; 36: 227-236.
- [25] Kordeli E, Lambert S and Bennett V. AnkyrinG: a new ankyrin gene with neural-specific isoforms localized at the axonal initial segment and node of Ranvier. *J Biol Chem* 1995; 270: 2352-2359.
- [26] Leterrier C. The axon initial segment: an updated viewpoint. *J Neurosci* 2018; 38: 2135-2145.

## Connexin36 at axon initial segments

- [27] Lariviere RC and Julien JP. Functions of intermediate filaments in neuronal development and disease. *J Neurobiol* 2004; 58: 131-48.
- [28] Clarke WT, Edwards B, McCullagh KJ, Kemp MW, Moorwood C, Sherman DL, Burgess M and Davies KE. Syncoilin modulates peripheral filament networks and is necessary for large-calibre motor neurons. *J Cell Sci* 2010; 123: 2543-2552.
- [29] Bautista W, Nagy JI, Dai Y and McCrea DA. Requirement of neuronal connexin36 in pathways mediating presynaptic inhibition of primary afferents in functionally mature mouse spinal cord. *J Physiol* 2012; 590: 3821-39.
- [30] Hervé JC, Derangeon M, Sarrouilhe D and Bourmeyster N. Influence of the scaffolding protein zonula occludens (ZOs) on membrane channels. *Biochim Biophys Acta* 2014; 1838: 595-604.
- [31] Lynn BD, Li X and Nagy JI. Under construction: Building the macromolecular superstructure and signaling components of an electrical synapse. *J Membr Biol* 2012; 245: 303-317.
- [32] Bender KJ and Trussell LO. The physiology of the axon initial segment. *Annu Rev Neurosci* 2012; 35: 249-65.
- [33] Huang CY and Rasband MN. Axon initial segments: structure, function and disease. *Ann NY Acad Sci* 2018; 1420: 46-61.
- [34] Fukuda J. Network architecture of gap junction-coupled neuronal linkage in the striatum. *J Neurosci* 2009; 29: 1235-1243.
- [35] Shigematsu N, Nishi A and Fukuda T. Gap junctions interconnect different subtypes of parvalbumin-positive interneurons in barrels and septa with connectivity unique to each subtype. *Cereb Cortex* 2019; 29: 1414-1429.
- [36] Nagy JI, Bautista W, Blakley B and Rash JE. Morphologically mixed chemical-electrical synapses formed by primary afferents in rodent vestibular nuclei as revealed by immunofluorescence detection of connexin36 and vesicular glutamate transporter-1. *Neuroscience* 2013; 252: 468-488.
- [37] Bennett MV and Zukin RS. Electrical coupling and neuronal synchronization in the mammalian brain. *Neuron* 2004; 41: 495-511.
- [38] Connors BW and Long MA. Electrical synapses in the mammalian brain. *Annu Rev Neurosci* 2004; 27: 393-418.
- [39] de Zeeuw CI, Ruigrok TJ, Holstege JC, Schalkamp MP and Voogd J. Intracellular labeling of neurons in the medial accessory olive of the cat: III. Ultrastructure of axon hillock and initial segment and their GABAergic innervation. *J Comp Neurol* 1990; 300: 495-510.
- [40] Nagy JI, Urena-Ramirez V and Ghia JE. Functional alterations in gut contractility after connexin36 ablation and evidence for gap junctions forming electrical synapses between nitrergic enteric neurons. *FEBS Letts* 2014; 588: 1480-90.
- [41] Shu Y, Duque A, Yu Y, Haider B and McCormick DA. Properties of action-potential initiation in neocortical pyramidal cells: evidence from whole cell axon recordings. *J Neurophysiol* 2007; 97: 746-760.
- [42] Draguhn A, Traub RD, Schmitz D and Jefferys JG. Electrical coupling underlies high-frequency oscillations in the hippocampus in vitro. *Nature* 1998; 394: 189-192.
- [43] Traub RD, Schmitz D, Jefferys JG and Draguhn A. High-frequency population oscillations are predicted to occur in hippocampal pyramidal neuronal networks interconnected by axo-axonal gap junctions. *Neuroscience* 1999; 92: 407-426.
- [44] Traub RD and Bibbig A. A model of high-frequency ripples in the hippocampus based on synaptic coupling plus axon-axon gap junctions between pyramidal neurons. *J Neurosci* 2000; 20: 2086-2093.
- [45] Simon A, Traub RD, Vladimirov N, Jenkins A, Nicholson C, Whittaker RG, Schofield I, Clowry GJ, Cunningham MO and Whittington MA. Gap junction networks can generate both ripple-like and fast ripple-like oscillations. *Eur J Neurosci* 2014; 39: 46-60.
- [46] Mercer A, Bannister AP and Thomson AM. Electrical coupling between pyramidal cells in adult cortical regions. *Brain Cell Biol* 2006; 35: 13-27.
- [47] Buhl DL, Harris KD, Hormuzdi SG, Monyer H and Buzsáki G. Selective impairment of hippocampal gamma oscillations in connexin-36 knock-out mouse in vivo. *J Neurosci* 2003; 23: 1013-1018.
- [48] Mathy A, Ho SS, Davie JT, Duguid IC, Clark BA and Häusser M. Encoding of oscillations by axonal bursts in inferior olive neurons. *Neuron* 2009; 62: 388-399.
- [49] Katzberg HD. Neurogenic muscle cramps. *J Neurol* 2015; 262: 1814-1821.

## Connexin36 at axon initial segments

**Supplementary Movie 1.** Maximum intensity projection of the image in **Figure 5B**, with 3D rotation showing maintained Cx36/AIS association at the various angles of rotation.